48th AIAA Aerospace Sciences Meeting Including the New Horizons Forum and Aerospace Exposition
4 - 7 January 2010, Orlando, Florida

AIAA 2010-1212

Analytic Hypersonic Aerodynamics for Conceptual Design of Entry Vehicles

Michael J. Grant* and Robert D. Braun†

Georgia Institute of Technology, Atlanta, GA, 30332

Capitalizing on the advances in symbolic manipulation technology, analytic hypersonic aerodynamic relations are developed based on Newtonian flow theory. Analytic relations for force coefficient, moment coefficient, and stability derivatives have been developed for basic shapes, including sharp cones, spherical segments, cylindrical segments, and flat plates at varying angles of attack and sideslip. Each basic shape has been generically parametrized, requiring the development of only a single set of analytic relations for each basic shape. These basic shapes can be superimposed to form common entry vehicles, such as sphere-cones and blunted biconics. Using Bezier curves of revolution, more general bodies of revolution are studied in which the location of the control nodes that define the shape of the curve is also generically parametrized. Analytic relations at unshadowed total angles of attack have been developed for these configurations. Analytic aerodynamic equations are orders of magnitude faster than commonly used panel methods and were validated using the NASA-developed Configuration Based Aerodynamics tool. Consequently, rapid aerodynamic trades and shape optimization can be performed. Additionally, the relations may impact guidance design using onboard trajectory propagation, real-time ablation modeling in simulations, and simultaneous vehicle-trajectory optimization.

Nomenclature

APAS	Aerodynamic Preliminary Analysis System
CBAERO	Configuration Based Aerodynamics
CFD	Computational Fluid Dynamics
HABP	Hypersonic Arbitrary Body Program
A_{ref}	Reference area
$\mathbf{B}$	Control node location of Bezier curve
C_A	Axial force coefficient
C'_A	Axial force coefficient in total angle of attack frame
C_l	Moment coefficient about x-axis
C_m	Moment coefficient about y-axis
$C_{m,\alpha}$	Pitch moment stiffness
C_n	Moment coefficient about z-axis
C_p	Pressure coefficient
C_N	Normal force coefficient
C'_N	Normal force coefficient in total angle of attack frame
$C_{N,\beta}$	Yaw moment stiffness
C_S	Side force coefficient
C_X	Force coefficient in x-direction
C_Y	Force coefficient in y-direction
C_Z	Force coefficient in z-direction

*Graduate Research Assistant, Guggenheim School of Aerospace Engineering, AIAA Student Member.

†David and Andrew Lewis Associate Professor of Space Technology, Guggenheim School of Aerospace Engineering, AIAA Fellow

d	Base diameter of conic section
dA	Differential area element
dA_{planar}	Differential area projected on y-z plane
$\mathbf{df}$	Differential force from Newtonian flow
h	Height of conic section
l_{ref}	Reference length
L	Length of cone
L/D	Lift to drag ratio
n	Order of Bezier curve
$\hat{\mathbf{n}}$	Inward unit normal
p	Pressure
p_∞	Freestream pressure
P	Bezier curve function
$\mathbf{r}$	Position vector of differential element
r_n	Nose radius
t	Normalized arclength of Bezier curve
u	Surface parametrization variable
v	Surface parametrization variable
$\mathbf{V}_\infty$	Freestream velocity vector
α	Angle of attack
β	Sideslip
δ	Blended wedge half-angle
δ_c	Cone half-angle
δ_1	Forward conic half-angle
δ_2	Aft conic half-angle
ΔA	Area of panel
ϵ	Total effective angle of attack
θ	Local body inclination relative to freestream direction
ρ_∞	Freestream density
ϕ'	Angle between the body frame and total angle of attack frame

I. Introduction

TRADITIONALLY, during the design of entry vehicles, it is difficult to simultaneously account for all major disciplines due to the computational requirements of high fidelity code. Consequently, a time consuming iterative process is typically employed using a large team in which members separately analyze each discipline. For example, computational fluid dynamics (CFD) is used to obtain the hypersonic aerodynamics of various entry vehicles. Due to the substantial computational requirements of CFD, vehicles are generally chosen that provide the necessary aerodynamic performance, such as L/D and ballistic coefficient, to accomplish a given mission. Subsequently, the vehicle is designed to meet these performance constraints.

During conceptual design, methods are typically employed to improve computational speed at the expense of a small reduction in fidelity. For example, panel methods can be used in conjunction with Newtonian flow theory to obtain the hypersonic aerodynamic characteristics of a vehicle with orders of magnitude reduction in computational requirements compared to CFD. Panel methods are widely used during conceptual design due to the ability of these methods to rapidly evaluate arbitrary shapes. Although panel methods are much faster than CFD, the designer is still required to limit the number of vehicle shapes analyzed due to the relatively high remaining computational requirements, for example when compared to trajectory propagation, during the generation of aerodynamic coefficient tables. Consequently, a fixed vehicle is usually chosen prior to trajectory design. Once the trajectory has been designed for the given vehicle, an iterative process is performed to alter the vehicle dimensions and, consequently, the aerodynamic characteristics, to accomplish the desired mission.

If a further reduction in aerodynamic computational requirements near that of trajectory propagation could be achieved, then the designer would have the ability to rapidly trade trajectory and vehicle design

parameters simultaneously. This would allow multidisciplinary design methods to be used for more comprehensive design space exploration. For hypersonic flight, this reduction in computational requirements could be achieved by obtaining analytic aerodynamic coefficients using Newtonian flow theory.

II. Newtonian Aerodynamic Theory

II.A. Motivation

In 1687, Issac Newton postulated that fluid flow can be viewed as a system of particles traveling in rectilinear motion as described in Propositions 34 and 35 of the *Principia*.[1] Newton assumed that when a particle strikes a surface, all of the momentum normal to the surface would be lost and all momentum tangential to the surface would be conserved as shown in Figure 1. Consequently, the pressure exerted by the fluid on the surface of a body is assumed to be solely originating from this loss of momentum normal to the surface. Under these assumptions, the nondimensional pressure coefficient, C_p, at any point on the surface of a body can be obtained from the Newtonian sine-squared relation shown in Eq. (1). Thus, the solution to the hypersonic aerodynamics problem is mapped to a geometry problem. Furthermore, the pressure exerted by the fluid on any portion of the surface not directly exposed to the flow, denoted as the shadowed region of a body, is assumed to be equivalent to the freestream pressure in which the motion of the fluid does not influence the pressure in this region. Thus, $C_p = 0$ throughout the shadowed region as shown in Figure 2.[2]

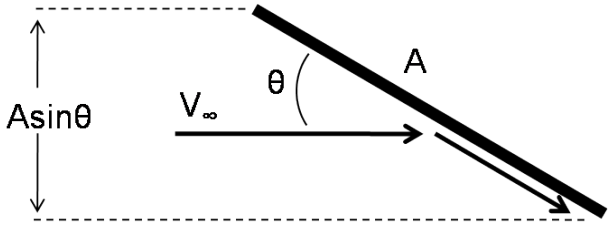

Figure 1. Momentum Transfer of Particle on Inclined Surface.[2]

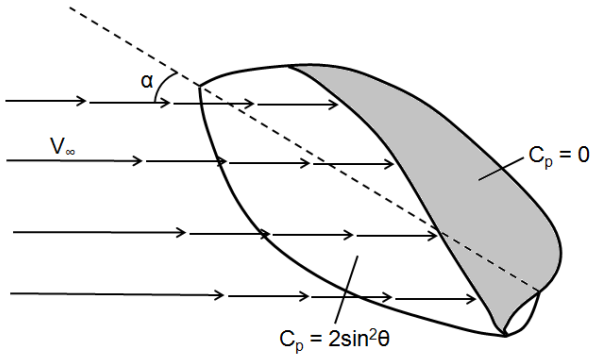

Figure 2. Example of Shadowed Body.[2]

$$C_p = \frac{p - p_\infty}{\frac{1}{2}\rho_\infty V_\infty^2} = 2\sin^2\theta \tag{1}$$

Newton originally applied his theory to model the pressure on the walls of a water channel. Experimental tests performed by d'Alembert later concluded that this model is inaccurate for subsonic flow conditions. However, as the Mach number increases to hypersonic speeds, the shock wave approaches the surface of the body. Thus, as the flow velocity changes direction after crossing the shock, the flow appears to be deflected by the body similar to Newtonian flow theory as shown in Figure 1. Furthermore, as the Mach number continues to increase, the shock continues to approach the body surface. Thus, as Mach number increases, Newtonian flow theory improves in accuracy and the aerodynamic coefficients are computed independent of Mach number. In conceptual design applications, the Mach independence principle allows for the fast computation of aerodynamic coefficients using the pressure coefficient in Eq. (1) at hypersonic speeds.[2]

II.B. Application of Newtonian Flow Theory

In order to calculate the aerodynamic coefficients of a hypersonic vehicle, a surface integral of C_p must be calculated. As previously mentioned, the pressure exerted on the vehicle is due to the total loss of momentum in the direction normal to the surface. Thus, the pressure coefficient, C_p, exerted over a differential element on the surface of a vehicle, dA, results in a differential force, $\mathbf{df}$, imparted on the vehicle in the inward unit normal direction of the surface, $\hat{\mathbf{n}}$, as shown in Eq. (2). Using conventional aircraft body axes shown in Figure 3 and corresponding freestream velocity vector, $\mathbf{V}_\infty$, shown in Eq. (3) as function of angle of attack, α, and sideslip, β, the aerodynamic force coefficients along the body axes, C_X, C_Y, and C_Z, can be calculated

through surface integration of the differential force in the x, y, and z directions as shown in Eq. (4). The axial force coefficient, C_A, side force coefficient, C_S, and normal force coefficient, C_N, commonly used in entry vehicle applications is related to the aerodynamic force coefficients along the body axes as shown in Eq. (4). The corresponding moment coefficients about the body axes, C_l, C_m, and C_n, are computed relative to the origin of the body axes as shown in Eq. (5), where $\mathbf{r}$ is the position vector of the differential area element. Furthermore, pitch and yaw stability derivatives can be calculated using Eq. (6) and Eq. (7).

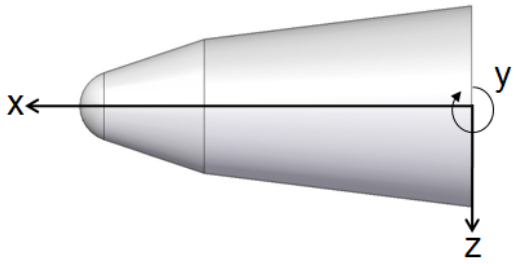

Figure 3. Body Axes Definition.

$$\mathbf{df} = C_p \, \hat{\mathbf{n}} \, dA \tag{2}$$

$$\mathbf{V}_\infty = [-\cos(\alpha)\cos(\beta) \quad -\sin(\beta) \quad -\sin(\alpha)\cos(\beta)]^T \tag{3}$$

$$\begin{bmatrix} C_X \\ C_Y \\ C_Z \end{bmatrix} = \begin{bmatrix} -C_A \\ C_S \\ -C_N \end{bmatrix} = \frac{1}{A_{ref}} \iint_S \begin{bmatrix} \mathbf{df}^T\hat{\mathbf{x}} \\ \mathbf{df}^T\hat{\mathbf{y}} \\ \mathbf{df}^T\hat{\mathbf{z}} \end{bmatrix} = \frac{1}{A_{ref}} \iint_S C_p \begin{bmatrix} \mathbf{n}^T\hat{\mathbf{x}} \\ \mathbf{n}^T\hat{\mathbf{y}} \\ \mathbf{n}^T\hat{\mathbf{z}} \end{bmatrix} dA \tag{4}$$

$$\begin{bmatrix} C_l \\ C_m \\ C_n \end{bmatrix} = \frac{1}{A_{ref} \cdot l_{ref}} \iint_S \begin{bmatrix} (\mathbf{r}\times\mathbf{df})^T\hat{\mathbf{x}} \\ (\mathbf{r}\times\mathbf{df})^T\hat{\mathbf{y}} \\ (\mathbf{r}\times\mathbf{df})^T\hat{\mathbf{z}} \end{bmatrix} = \frac{1}{A_{ref} \cdot l_{ref}} \iint_S C_p \begin{bmatrix} (\mathbf{r}\times\mathbf{n})^T\hat{\mathbf{x}} \\ (\mathbf{r}\times\mathbf{n})^T\hat{\mathbf{y}} \\ (\mathbf{r}\times\mathbf{n})^T\hat{\mathbf{z}} \end{bmatrix} dA \tag{5}$$

$$C_{m,\alpha} = \frac{\partial C_m}{\partial \alpha} \tag{6}$$

$$C_{n,\beta} = \frac{\partial C_n}{\partial \beta} \tag{7}$$

Newtonian flow theory provides a first-order, computationally efficient means in which the hypersonic aerodynamics of various vehicle geometries can be obtained. Newtonian aerodynamic theory is an excellent approximation for the conceptual design of slender bodies in which the shock wave is in the vicinity of the surface of the body. However, this traditional Newtonian flow theory is typically modified for blunt bodies in which a normal shock resides upstream of the vehicle.[3] Such a modification has led to the development of the Modified Newtonian theory in which the leading 2 in Eq. (1) is reduced to account for the pressure loss across the normal shock. The results detailed in this report assume traditional Newtonian flow in which the leading 2 is maintained. However, should the use of Modified Newtonian flow theory be required, the analytic results in this report can be scaled by the appropriate multiplier.

III. Calculation of Hypersonic Aerodynamics Using Newtonian Flow Theory

As previously mentioned, the calculation of aerodynamic coefficients at hypersonic speeds requires the integration of C_p over the surface of the vehicle. Portions of the vehicle surface shadowed from the flow are assumed to have a $C_p = 0$. Thus, the integration of C_p need only be computed over the unshadowed surface of the vehicle.

III.A. Panel Methods and CBAERO

Currently, the surface integration required by Newtonian flow theory is performed numerically using panel methods that approximate the shape of a vehicle using small flat plates. Thus, the integration is approximated as a finite summation of the integrand over the flat plates approximating the shape of the vehicle. For example, the approximation of C_X is shown in Eq. (8), where ΔA is the area of each panel. This numerical approximation is a source of error in the Newtonian estimate.

$$C_X \approx \frac{1}{A_{ref}} \sum_{i=0}^{N} C_p \, \mathbf{n}^T \hat{\mathbf{x}} \, \Delta A \tag{8}$$

Many paneling codes have been developed, including the Hypersonic Arbitrary Body Program (HABP) in conjunction with the Aerodynamic Preliminary Analysis System (APAS) developed in the late 1970s and early 1980s and the Configuration Based Aerodynamics (CBAERO) tool developed in the past decade.[4–7] CBAERO serves as a means to verify the analytic relations developed in this work. The results of the CBAERO Modified Newtonian calculations are properly scaled to account for the difference in theory.

CBAERO provides a straightforward methodology to compute the aerodynamic coefficients of relatively complicated geometries. The process required for CBAERO is the following:

1.) Construct a mesh of the vehicle describing the nodes and corresponding flat plates. The construction of a mesh for complicated shapes would require modeling in a CAD package. Bodies of revolution can be meshed fairly easily using automated routines.

2.) Calculate the unit inward normal and C_p for each panel. Any panel with a unit inward normal in the opposite direction from the flow is ignored since it is shadowed, resulting in $C_p = 0$.

3.) Calculate the aerodynamic forces through numerical integration of C_p over the surface of the vehicle and generate tables of aerodynamic coefficients for various α and β.

This process must be repeated for any change in the shape of the vehicle. Although CBAERO allows for rapid aerodynamic calculations when compared to CFD, the construction of aerodynamic tables remains slow compared to other disciplines of the design process, such as trajectory propagation. Additionally, the resolution of the mesh must be addressed when using panel methods. The number of required panels to achieve a desired accuracy in the approximate surface integral solution is generally unknown in the beginning of the meshing process. Consequently, multiple meshes of various resolution must be evaluated until convergence of aerodynamic coefficients is observed. Furthermore, the construction of meshes in CAD packages limit the ability to automate entry vehicle shape change necessary for parametric analysis and optimization. These time-consuming issues associated with panel methods limit the number of shapes analyzed during entry vehicle design.

III.B. Motivation for Analytic Hypersonic Aerodynamics

While panel methods, such as CBAERO, would likely be required for the conceptual design of complicated geometries such as the Space Shuttle Orbiter, X-38, HL-20, and others, many entry vehicle shapes used in previous and current mission studies are not complex. For example, all previous and currently planned Mars missions have used a blunt sphere-cone. Various human Mars mission studies have used blunt sphere-cones and blunted biconics.[8–10] The Stardust and Genesis Earth entries also used a blunt sphere-cone.[11,12] Additionally, the Apollo command module and planned Orion command module both utilize a spherical forebody. Many high performance military entry vehicles are slender sphere-cones and slender biconics with minor nose blunting to account for extreme heating environments. Alternative high performance entry vehicles include blended wedge designs, such as the SHARP L1, that consist of flat plates, conical frustums, and nose blunting through a cylindrical segment.[13]

The surface geometry of these basic shapes, along with additional complex shapes, can be expressed analytically. Consequently, the solution to the geometric problem of Newtonian flow theory, *i.e.*, the surface integration in Eq. (4) and Eq. (5), can also be performed analytically. The resulting analytic relations provide exact Newtonian aerodynamic coefficients instead of the approximate Newtonian aerodynamic coefficients obtained from panel methods. Additionally, the evaluation of the resulting analytic relations would be nearly instantaneous, allowing for rapid conceptual design and/or simultaneous entry vehicle and trajectory optimization that is not currently practical when using panel methods.

IV. Analytic Hypersonic Aerodynamics Overview

IV.A. Historical Overview

IV.A.1. Basic Shapes

Due to the absence of digital computers, analytic hypersonic aerodynamic coefficients based on Newtonian flow theory were developed in the late 1950s and early 1960s. This early work[14] focused on developing analytic aerodynamic relations that could be processed through a computer to develop large aerodynamic tables of various vehicle configurations that consisted of basic shapes. These large tables could then be used by hand to quickly estimate aerodynamic characteristics of various sharp and blunted circular conics or elliptical conics at various angles of attack and sideslip. Comparisons were also made to hypersonic experimental data which showed good agreement with the theory while maintaining trends as desired for conceptual design.

IV.A.2. Historical Bodies of Revolution

Newtonian flow theory had also been applied in the past to generic bodies of revolution. Variational methods[15] have been used at zero angle of attack to determine optimal profiles to minimize the pressure drag of Newtonian flow theory for various geometric constraints.[16,17] The resulting minimum drag bodies of revolution from this work are shown in Figure 4. In order to accommodate nonzero angles of attack, generic bodies of revolution were approximated as a series of open rings at various stations along the axis of revolution.[18–21] In this work, focus was given to the development of charts or tables that could be used to develop aerodynamic coefficients by numerically evaluating the local inclination of each ring relative to the axis of revolution.

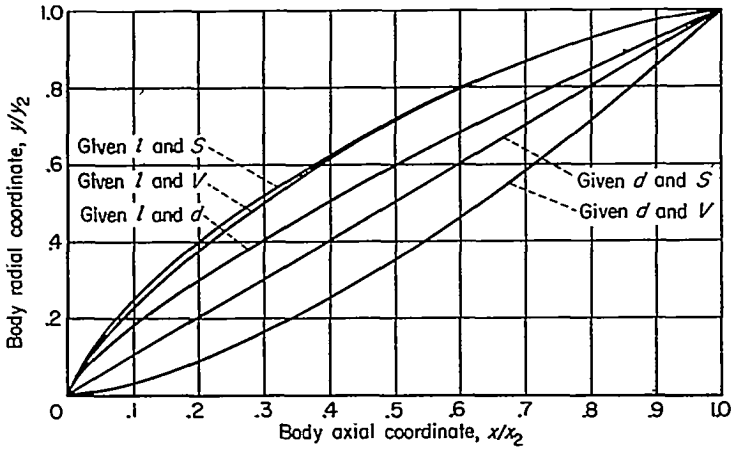

Figure 4. Minimum Drag Bodies of Revolution for Various Geometric Constraints.[16]

IV.A.3. Absence of Analytic Hypersonic Aerodynamics in Present-Day Analyses

The analytic relations developed in the 1950s and 1960s have largely been unnoticed by the aerospace community in the recent decades. The manual development of analytic relations is time-intensive and requires complex integrations to be performed. Hence, the integration process is largely dependent on integral tables and appropriate substitutions, a prohibitive process during conceptual design. Consequently, the advent of the digital computer resulted in the widespread adoption of panel and CFD methods over analytic relations. This can be observed by the many recent shape design studies that employ panel methods.[22,23] While the ability of these methods to model general and complicated shapes, such as the Space Shuttle Orbiter, are desirable, these methods are orders of magnitude slower than evaluating analytic aerodynamic equations. Consequently, the computational requirements of present-day panel methods have limited the number of shapes evaluated during conceptual design.

Analytic hypersonic relations would allow many shapes to be evaluated rapidly. Additionally, if each basic shape is parametrized to construct a family of similar shapes, then each analytic relation would only have to

be developed once. This is a major advantage over panel methods that must be executed each time the shape of the vehicle changes. Furthermore, advances in symbolic manipulation tools, such as Mathematica[24] and Maple,[25] allow for the development of an automated process to develop analytic relations for many shapes. This process has been generalized to allow for the integration of many shapes regardless of how the surface is parametrized.

IV.B. Process for Development of Analytic Relations

An integrated Matlab and Mathematica environment has been constructed to automate the development of analytic relations for user-supplied shapes. Matlab is used to drive the process and employs Mathematica's symbolic engine to perform the integrations. Mathematica was chosen due to its ability to add constraints on symbolic variables (for example, the radius of a sphere is always greater than zero). Supplying this information to Mathematica as an assumption influences how the integration is performed. After the designer describes the surface of the shape, routines containing the analytic aerodynamic relations are generated in a Matlab-based aerodynamics module. This module can be easily integrated into trajectory simulations, be used for parametric analyses, or be used in shape optimization. The six steps performed in this automated process are further detailed.

Step 1: Surface Parametrization

The analytic aerodynamic expressions are obtained by integrating C_p over the unshadowed surface of the vehicle as described in Eq. (4) and Eq. (5). In order to evaluate these integrals, the surface of each shape must be parametrized by two independent variables via a position vector, $\mathbf{r}$, as shown in Eq. (9), where $f(u,v)$, $g(u,v)$, and $h(u,v)$ describe the x, y, and z location of a point on the surface of the vehicle as a function of the surface parametrization (u,v). The choice in parametrization variables, u and v, is largely at the discretion of the designer. However, the choice in parametrization can dramatically influence the ability of Mathematica to obtain closed-form solutions when performing the integrations. Additionally, due to the convention used when computing the surface normal, u and v must be chosen such that $\mathbf{r}_u \times \mathbf{r}_v$ is pointed inward, where $\mathbf{r}_u = \frac{\partial \mathbf{r}}{\partial u}$ and $\mathbf{r}_v = \frac{\partial \mathbf{r}}{\partial v}$. The choice in parametrization also influences the expression for the differential area, dA, of the integrations. The differential area element is computed using the magnitude of the inward normal vector as shown in Eq. (10).

$$\mathbf{r} = [f(u,v) \quad g(u,v) \quad h(u,v)]^T \tag{9}$$

$$dA = \| \mathbf{n} \| = \| \mathbf{r}_u \times \mathbf{r}_v \| \tag{10}$$

Step 2: Compute Pressure Coefficient

With the surface parametrized by u and v, the pressure coefficient can be computed. Recall from Figure 1 that $\sin(\theta)$ is defined as shown in Eq. (11), where $\hat{\mathbf{n}}$ is calculated from Eq. (12) and $\mathbf{V}_\infty$ is defined in Eq. (3) of Section II.B. With $\sin(\theta)$ known, C_p can be computed using Eq. (1).

$$\sin(\theta) = \hat{\mathbf{V}}_\infty^T \hat{\mathbf{n}} \tag{11}$$

$$\hat{\mathbf{n}} = \frac{\mathbf{r_u} \times \mathbf{r_v}}{\| \mathbf{r_u} \times \mathbf{r_v} \|} \tag{12}$$

Step 3: Compute Shadow Boundary

The major challenge in deriving analytic aerodynamic expressions is ensuring that the integration is not performed over shadowed regions of the vehicle where $C_p = 0$. With an analytic expression for $\sin(\theta)$, the shadow boundary can be computed by solving $\sin(\theta) = 0$ for v as a function of u since the surface integration is first performed with respect to v. Note that the solution to this equation may have multiple results, especially if the surface is parametrized with trigonometric functions. A numerical test is performed to determine which solutions should be incorporated as the lower and upper bounds. Note that the limits of integration are a function of vehicle shape and flow direction. Only convex shapes are currently supported.

This allows the limits of integration in v to be defined by the solution of $\sin(\theta) = 0$. If the shape was not convex, then shadowed regions may have boundaries where $\sin(\theta) \neq 0$.

Step 4: Compute Reference Values

The reference area and reference length for each shape is computed based on the parametrization used. The reference area is computed as the projected area of the shape on the y-z plane using Eq. (13) assuming $\alpha = \beta = 0$, where dA_{planar} is the incremental area projected on the y-z plane. Since $\mathbf{r}_u \times \mathbf{r}_v$ represents the inward normal of a convex shape and dA_{planar} must be positive to obtain a positive reference area, dA_{planar} is computed using Eq. (14). Due to the convexity requirement of the shape, the entire surface is unshadowed at $\alpha = \beta = 0$, and, consequently, the limits of integration must be chosen to span the entire surface of the shape. The reference length is computed as the maximum span of the vehicle in the x-direction.

$$A_{ref} = \int_{u_{min}}^{u_{max}} \int_{v_{min}}^{v_{max}} dA_{planar} \tag{13}$$

$$dA_{planar} = (\mathbf{r}_u \times \mathbf{r}_v)^T(-\hat{\mathbf{x}}) \tag{14}$$

Step 5: Evaluate Surface Integral

The aerodynamic coefficients are computed by evaluating the surface integral in Eq. (4) and Eq. (5). The first integration is performed with respect to v since the shadow boundary was solved as $v = v(u)$. After the integration is performed with respect to v, the shadow boundaries are substituted as the limits of integration for v. The remaining integrand is only a function of u, and the second integration is performed with respect to u. The limits of integration substituted for u are constants, u_1 and u_2. During evaluation of the analytic expressions, the designer specifies the portion of the shape used by supplying the values for u_1 and u_2.

Step 6: Output Aerodynamics Code

After the analytic relations have been developed, they are output to a Matlab-based aerodynamics module. This module contains the analytic relations, reference area, and reference length. Hence, as the analytic relations of various shapes are developed, the aerodynamics module becomes a library containing analytic relations for a wide variety of shapes.

V. Derivation and Validation of Analytic Expressions for Basic Shapes

The shape of common entry vehicles can be constructed via the superposition of basic shapes. The construction and parametrization of the various basic shapes will be shown. It is important to note that all basic shapes are parametrized by variables describing the family of the basic shape, such as the half-angle of a sharp cone, and by variables describing the surface, u and v, as previously described. This generalization of each basic shape allows the development of only one set of analytic relations for each basic shape family. Each basic shape is chosen to have symmetry along the body axes where applicable and be centered at the origin. A range of angles of attack and sideslip was chosen to validate both shadowed and unshadowed angles of attack.

V.A. Sharp Cone Family

Although sharp cones are not used alone as entry vehicles due to the significant heating that would occur on the sharp nose, conical frustums are commonly used as portions of entry vehicles such as sphere-cones and biconics. The sharp cone family is parametrized by the cone half-angle, δ_c, and length along the axis of revolution, L. The surface of the sharp cone is parametrized using the local radius from the axis of revolution, $u = r$, and revolution angle, $v = \omega$, as shown in Figure 5. The resulting parametrized position vector, $\mathbf{r}$, is shown in Eq. (15).

$$\mathbf{r} = [L - \frac{u}{\tan(\delta)} \quad u\cos(v) \quad -u\sin(v)]^T \tag{15}$$

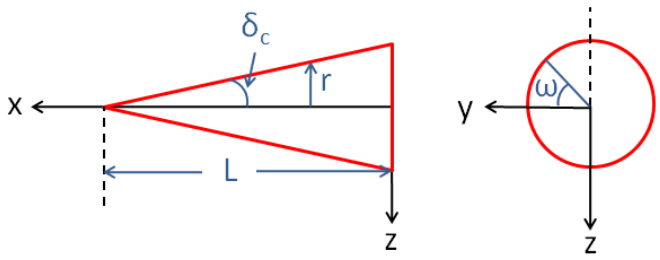

Figure 5. Side and Front View of Sharp Cone Parametrization.

Comparisons between the analytic relations and CBAERO in both force and moment coefficients for a 20^o sideslip and various cone half angles and angles of attack are shown in Figure 6 and Figure 7, respectively. Initially, comparisons were also planned between the analytic stability derivatives and CBAERO. However, the CBAERO mesh resolution required to obtain accurate stability derivatives was prohibitive due to the presence of numerical noise. However, as shown in Figure 7, excellent agreement was observed between the analytic moment equations and CBAERO. Therefore, a comparison was made between the analytic stability derivatives and the finite difference of analytic moment coefficients (shown in Figure 8). As expected, excellent agreement is observed in all cases. Note that the roll moment, C_l, is identically zero as expected for axisymmetric bodies.

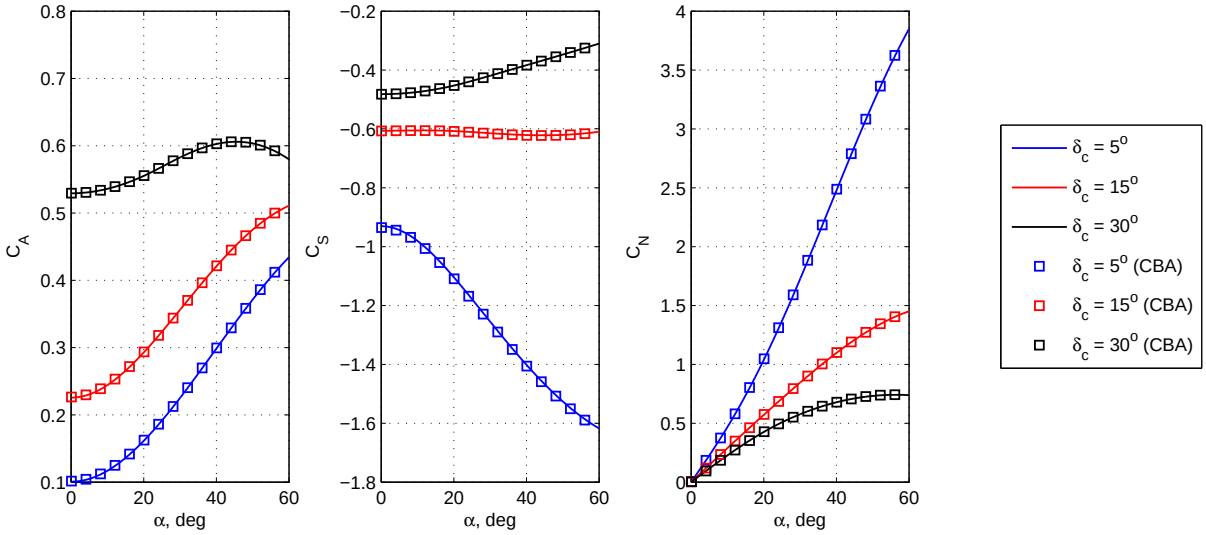

Figure 6. Sharp Cone Force Coefficient Validation, $\beta = 20^o$.

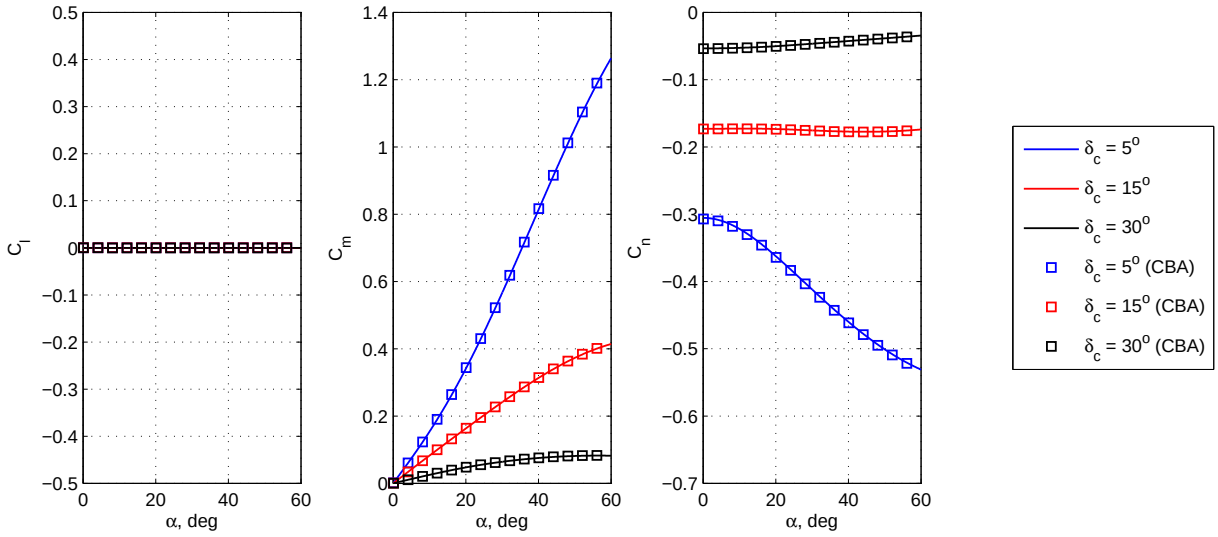

Figure 7. Sharp Cone Moment Coefficient Validation, $\beta = 20^o$.

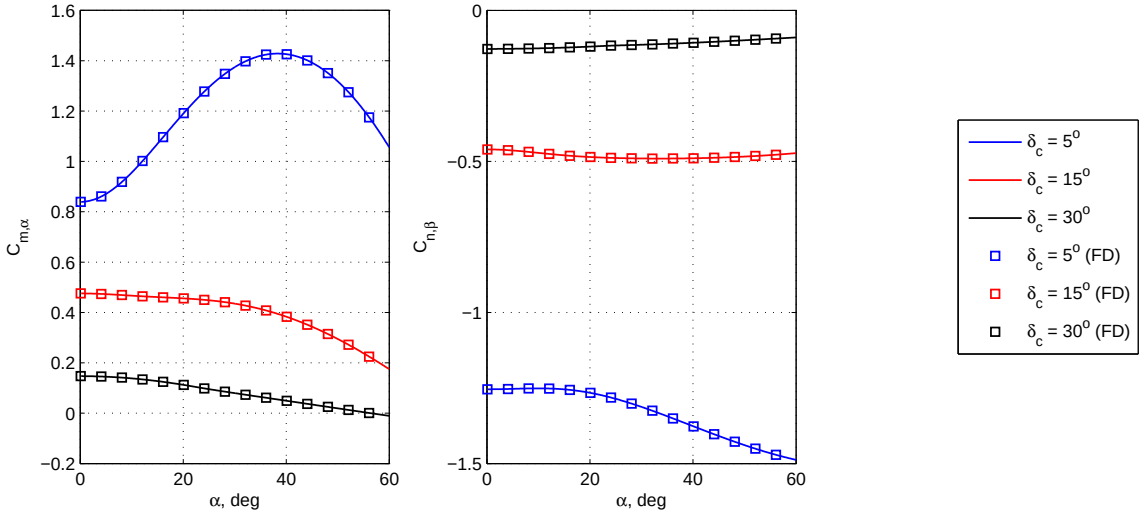

Figure 8. Sharp Cone Stability Derivative Validation, $\beta = 20^o$.

V.B. Spherical Segment Family

The blunting of entry vehicles to reduce aeroheating is often achieved through the addition of a spherical segment as the nose of the vehicle. For common entry vehicles such as sphere-cones and blunted biconics, the spherical segment family is parametrized by the nose radius, r_n, and cone half-angle, δ_c (Figure 9). The nose radius and cone half-angle determine the portion of the spherical segment used to blunt the vehicle due to tangency conditions enforced between the spherical segment and conical frustum. The surface of the spherical segment is parametrized by the distance from the origin along the x-axis, $u = x$, and revolution angle, $v = \omega$, as shown in Figure 9. The resulting position vector, $\mathbf{r}$, is shown in Eq. (16).

$$\mathbf{r} = [u \quad \sqrt{r_n^2 - u^2}\cos(v) \quad -\sqrt{r_n^2 - u^2}\sin(v)]^T \tag{16}$$

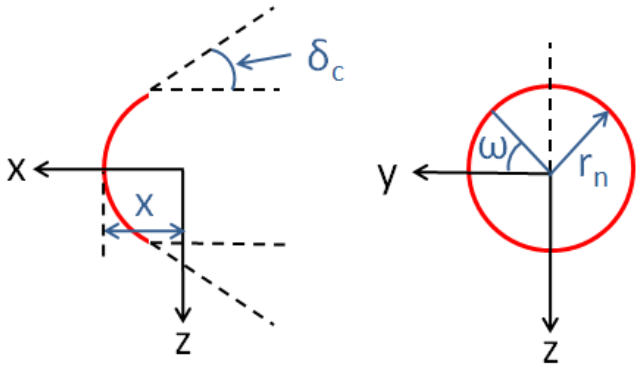

Figure 9. Side and Front View of Spherical Segment Parametrization.

In order to reduce the integration complexity associated with a spherical segment, analytic relations were derived using a total angle of attack, ϵ, that is a function of both angle of attack and sideslip as shown in Eq. (17). The resulting normal and axial force coefficients in the total angle of attack frame, C'_N and C'_A, are converted back to the body frame using Eq. (18), where ϕ' is the angle between the body frame and total angle of attack frame.[14] Comparisons between the analytic force coefficients and CBAERO for a 20^o sideslip and various half angles and angles of attack are shown in Figure 10. As shown, excellent agreement exists when using the total angle of attack formulation. Note that the distribution of Newtonian pressure forces always point to the center of the spherical segment. Thus, a spherical segment centered at the origin will exhibit no moments. This is confirmed by the solution of zero for all moments from the integration process. Consequently, no comparison is made between the moment coefficients and stability derivatives with CBAERO.

$$\epsilon = \arccos(\cos(\alpha)\cos(\beta)) \tag{17}$$

$$\begin{bmatrix} C_N \\ C_S \\ C_A \end{bmatrix} = \begin{bmatrix} C'_N \cos(\phi') \\ -C'_N \sin(\phi') \\ C'_A \end{bmatrix} \tag{18}$$

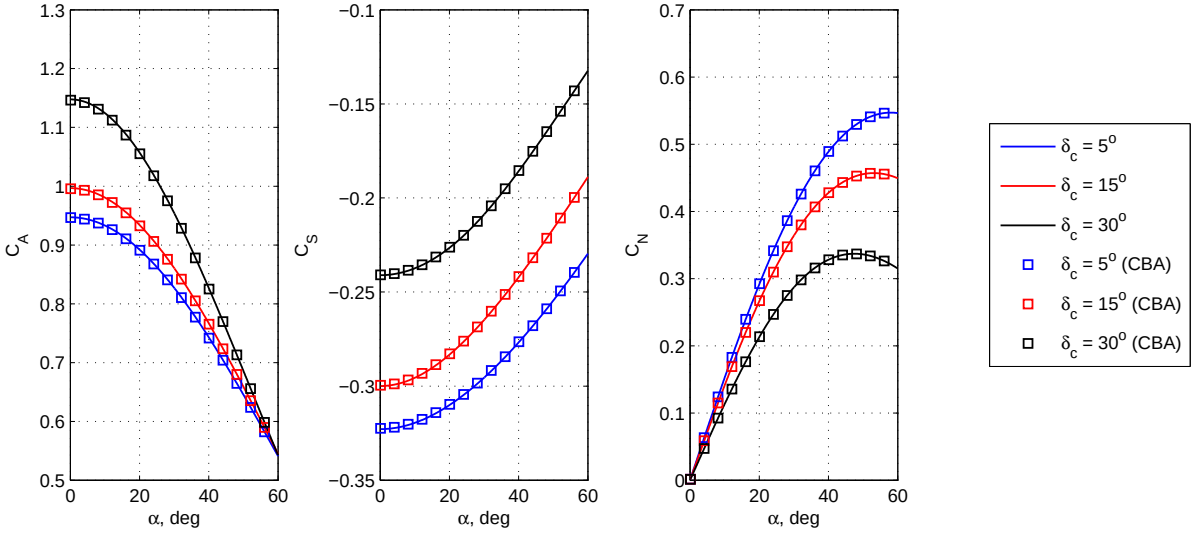

Figure 10. Spherical Segment Force Coefficient Validation, $\beta = 20^o$.

V.C. Flat Plate Family

Various portions of entry vehicles, such as stationary fins and moving control surfaces, can be approximated as flat plates. Additionally, the flat bodies of advanced entry vehicle concepts such as the blended wedge[13] can be modeled using flat plates. The flat plate family is parametrized by the half-angle of the blended wedge, δ, as shown in Figure 11.

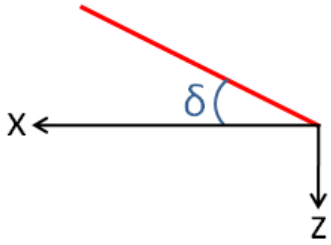

Figure 11. Side View of Flat Plate Parametrization.

According to Newtonian flow theory, the C_p distribution of a flat plate is constant. Thus, the force coefficients are obtained using Eq. (1), resulting in Eq. (19)-(21). Additionally, the moment coefficients about the centroid of the flat plate are identically zero. This is the simplest example of the form the analytic aerodynamics will appear. In general, a panel method approximates a shape as a collection of flat plates and does not provide a useful validation.

$$C_A = 2[\sin(\delta)\cos(\alpha)\cos(\beta) + \cos(\delta)\sin(\alpha)\cos(\beta)]^2 \sin(\delta) \tag{19}$$

$$C_S = 0 \tag{20}$$

$$C_N = 2[\sin(\delta)\cos(\alpha)\cos(\beta) + \cos(\delta)\sin(\alpha)\cos(\beta)]^2 \cos(\delta) \tag{21}$$

V.D. Cylindrical Segment Family

Although the cylindrical segment is not a common shape observed in entry vehicles, it is used to blunt advanced vehicle concepts such as the blended wedge.[13] The cylindrical segment family is parametrized by the nose radius, r_n, and blended wedge half-angle, δ. The nose radius and half-angle determine the portion of the cylindrical segment used to blunt the vehicle due to tangency conditions enforced between the spherical segment and flat plates of a blended wedge design. The surface of the cylindrical segment is parametrized by the distance from the origin along the y-axis, $u = y$, and revolution angle about the y-axis, $v = \theta$, as shown in Figure 12. The resulting position vector, $\mathbf{r}$, is shown in Eq. (22).

$$\mathbf{r} = [r_n \cos(v) \quad u \quad -r_n \sin(v)]^T \tag{22}$$

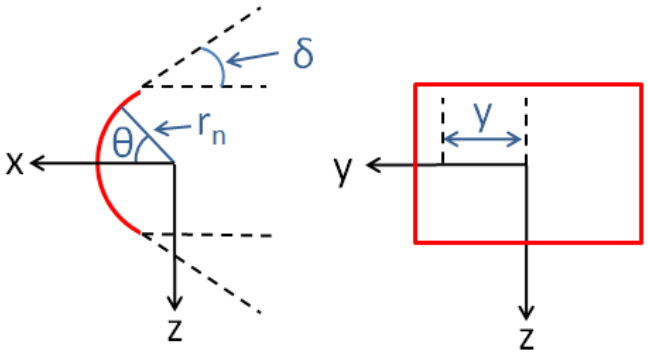

Figure 12. Side and Front View of Cylindrical Segment Parametrization.

In order to validate the cylindrical segment, a panel method based on the equations of a flat plate in Section V.C was developed. This allowed for easy verification of the aerodynamic coefficients since the construction of a vehicle in CBAERO is time consuming when the axis of revolution is not parallel to the flow at zero angle of attack and zero sideslip. Comparisons were made between the analytic force coefficients and the developed panel method for a 20^o sideslip and various half angles and angles of attack. As shown in Figure 13, excellent agreement exists between the cylindrical segment and the panel method. Note that the sideforce and moment coefficients of a cylinder centered at the origin are identically zero.

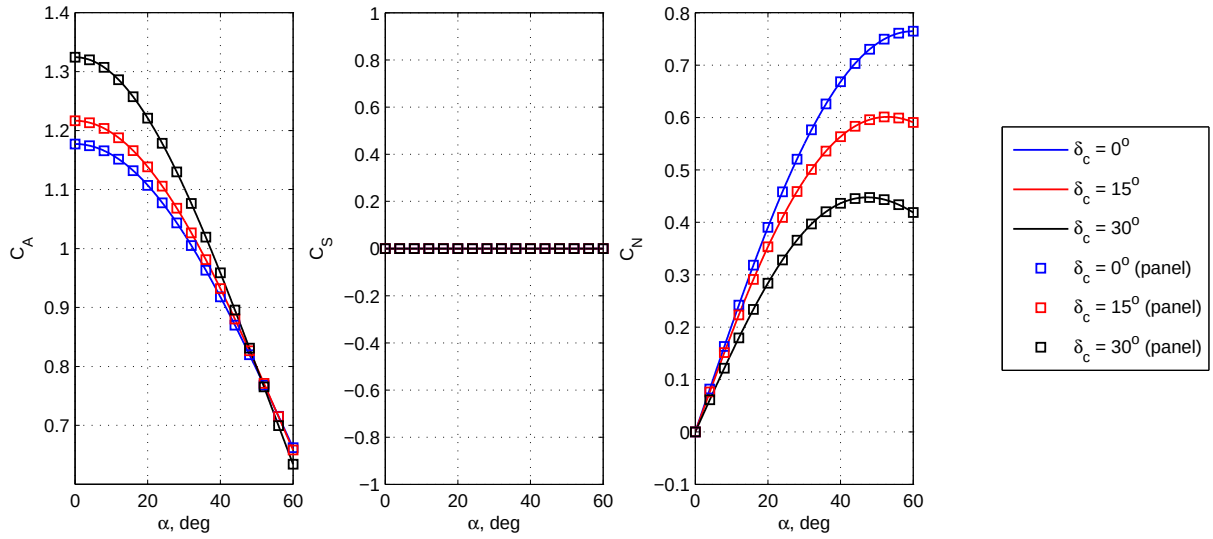

Figure 13. Cylindrical Segment Force Coefficient Validation, $\beta = 20^o$.

VI. Vehicle Construction Through Superposition

VI.A. Methodology

The aerodynamics of common entry vehicles can be determined through superposition of basic shapes. Sphere-cones can be constructed using a spherical segment and a single conical frustum, and biconics can be constructed using a spherical segment and two conical frustums. The geometry of a sphere-cone is specified by the nose radius, r_n, cone half angle, δ_1, and base diameter, d, as shown in Figure 14. The geometry of a blunted biconic is specified by the nose radius, r_n, forward cone half angle, δ_1, aft cone half angle, δ_2, base diameter, d, and height, h, as shown in Figure 15. Each basic shape used will likely have different reference areas and lengths. Therefore, the superpositioning of basic shapes cannot be performed by simply adding the aerodynamic coefficients from each shape. Rather, the aerodynamic coefficients of each basic shape must be scaled to a common reference area and length. For example, the axial force coefficient of a sphere-cone, $C_{A,sc}$, would be calculated using Eq. (23), where the overall vehicle reference area, A_{sc}, is chosen to be the base area of the sphere-cone.

$$C_{A,sc} = C_{A,cone}\frac{A_{ref,cone}}{A_{sc}} + C_{A,sphere}\frac{A_{ref,sphere}}{A_{sc}} \tag{23}$$

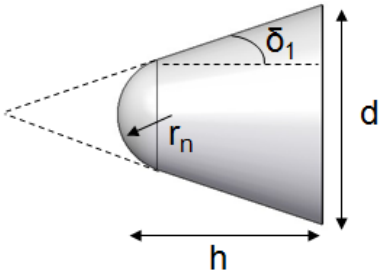

Figure 14. Sphere-Cone Parametrization.

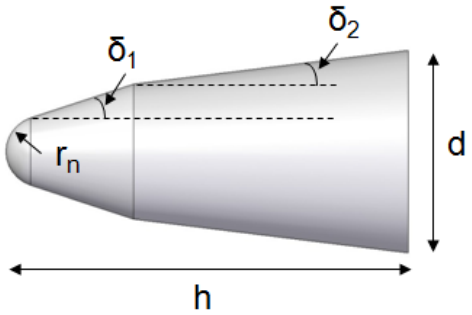

Figure 15. Biconic Parametrization.

VI.B. Sphere-Cone and Blunted Slender Biconic Validation

The force and moment coefficients for both a blunt sphere-cone and blunted slender biconic at a 20^o sideslip were validated with CBAERO using parameters listed in Table 1. As shown in Figure 16 and Figure 17, excellent agreement in force and moment coefficients is observed for both vehicles.

Table 1. Sphere-Cone and Blunted Biconic Parameters.

Parameter	*Sphere-Cone*	*Biconic*
r_n	0.3 ft.	1.0 in.
δ_1	70.0^o	17^o
δ_2	-	8^o
d	2.5 ft.	19.6 in.
h	-	48.0 in.

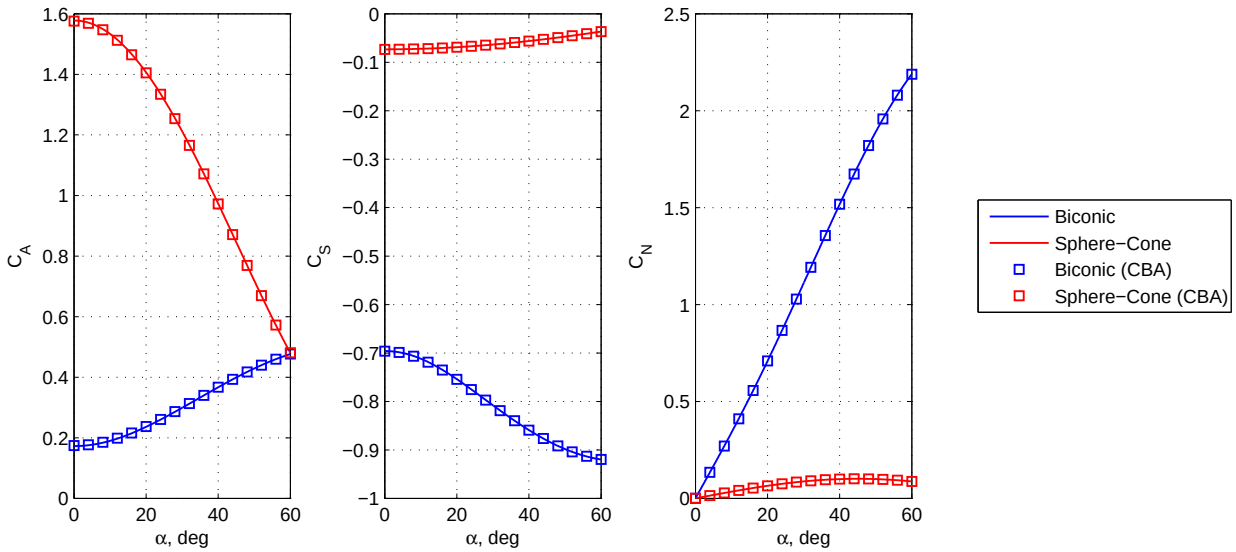

Figure 16. Sphere-Cone and Blunted Biconic Force Coefficient Validation, $\beta = 20°$.

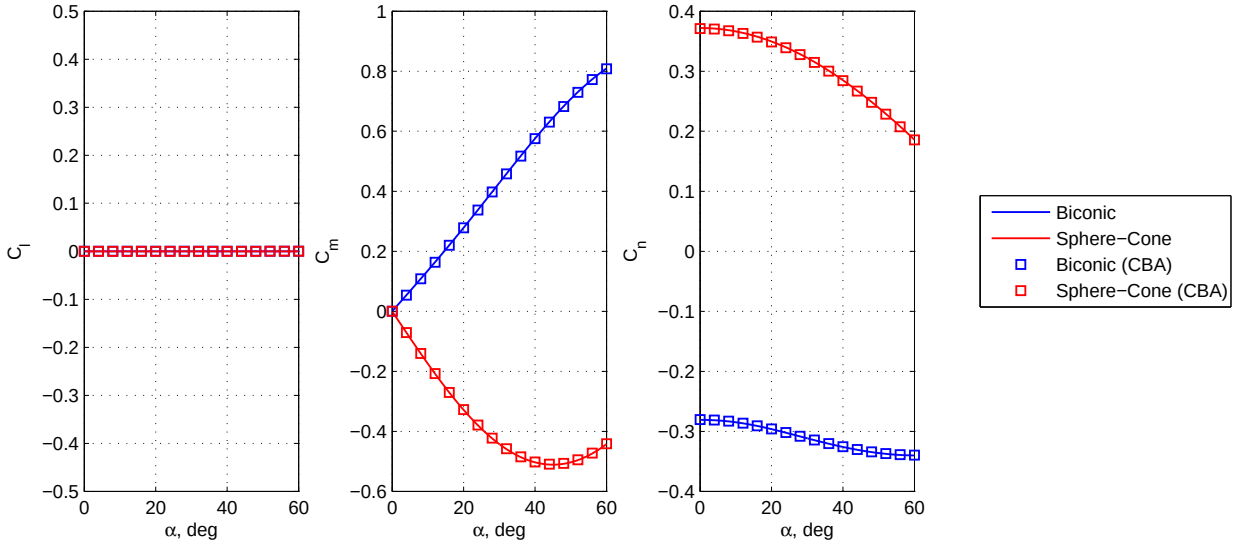

Figure 17. Sphere-Cone and Blunted Biconic Moment Coefficient Validation, $\beta = 20°$.

VI.C. Example Application Using the Superposition of Basic Shapes

As shown, basic shapes can be superpositioned to construct full entry bodies commonly used for various entry missions. The analytic relations allow for rapid parametric sweeps and shape optimization. As an example, vehicle designers may be interested in a biconic entry vehicle with a peak L/D of 2 subject to certain geometric constraints.

For this problem, a maximum vehicle height of 48 in. and a maximum base diameter of 21 in. was assumed. For a given diameter, an increase in the height would result in a more slender vehicle with higher peak L/D. Therefore, in order to maximize the base diameter, the height of the vehicle must also be maximized. Parametric sweeps over a wide range of angle of attack and zero sideslip were performed for various cone half angles, δ_1 and δ_2, in 1^o increments as well as various base diameters. Contours in peak L/D for the maximum allowable base diameter of 21 in. are shown in Figure 18. As shown, no sharp biconic is capable of achieving an L/D of 2. A theoretical best L/D of only 1.86 could be achieved with $\delta_1 = 18^o$ and $\delta_2 = 11^o$. Consequently, the base diameter was reduced until a sharp biconic with an L/D of 2 was identified. As shown in Figure 19, an L/D of 2 is achieved with $d = 19.6$, $\delta_1 = 17^o$, and $\delta_2 = 10^o$. Note that each point in the contour plots corresponds to a full sweep of angles of attack, a process that is reduced from hours using CBAERO to minutes using the analytic relations.

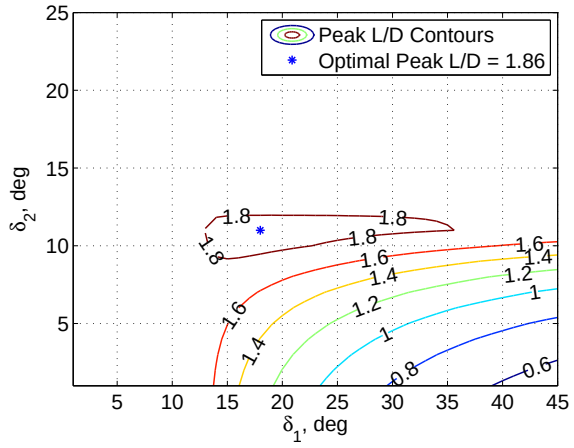

Figure 18. Contour of Peak L/D for d = 21 in.

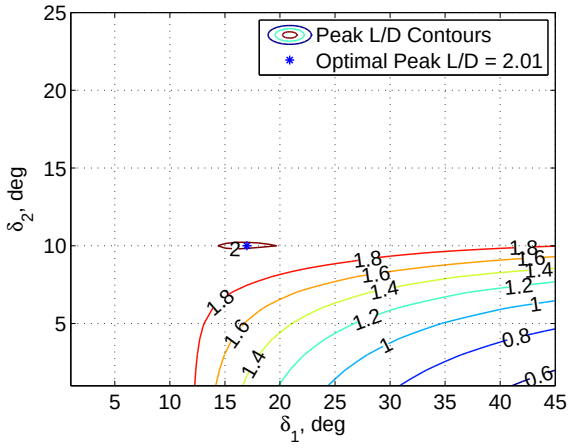

Figure 19. Contour of Peak L/D for d = 19.6 in.

VII. General Shapes

The superposition of basic shapes provides the capability to determine analytic aerodynamics of common entry vehicle shapes. However, shapes with improved aerodynamic performance outside of the range of basic shapes may be required to accomplish future missions. Therefore, it is desirable to be able to obtain the analytic aerodynamics of more general shapes. Many methods from computer-aided design exist to describe general shapes. As an initial step in this direction, analytic relations of low-order Bezier curves of revolution have been developed for unshadowed total angles of attack in which the full body is exposed to the flow.

VII.A. Bezier Curves of Revolution

The development of analytic relations for Bezier curves of revolution allow for rapid analysis of general bodies of revolution. The geometry of a Bezier curve is parametrized by a nondimensional arclength, t, as shown in Eq. (24), where $J_{n,i}(t)$ is shown in Eq. (25), $\binom{n}{i}$ is shown in Eq. (26), and $0 \leq t \leq 1$.[26] The location of the ith control node is specified in the vector $\mathbf{B_i}$ and the order of the Bezier curve is specified by n. The control nodes specify a control polygon inside which the Bezier curve must reside. The development of analytic relations was only performed for a second-order Bezier curve in which $n = 2$. Example Bezier curves, along with their corresponding control node locations and control polygons, are shown in Figure 20. As expected, each Bezier curve resides inside the control polygon and is connected to the initial and final control nodes.

$$\mathbf{P}(t) = \sum_{i=0}^{n} \mathbf{B_i}\ J_{n,i}(t) \tag{24}$$

$$J_{n,i}(t) = \binom{n}{i} t^i (1-t)^{n-i} \tag{25}$$

$$\binom{n}{i} = \frac{n!}{i!(n-i)!} \tag{26}$$

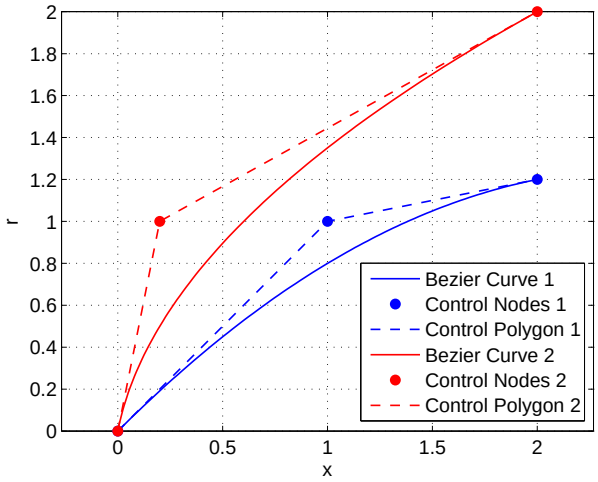

Figure 20. Bezier Curves of Revolution with Control Nodes and Control Polygons.

Analytic relations have been developed for a second-order Bezier curve of revolution in which the control node locations were generalized. This allows the development of one set of analytic relations to fully describe all second-order Bezier curves of revolution. These relations currently assume that the entire vehicle is exposed to the flow. Only analytic relations for the force coefficients have been developed to date. The force coefficients of the Bezier curves of revolution shown in Figure 20 have been validated with CBAERO as shown in Figure 21. As expected from Figure 20, Bezier curve 2 remains unshadowed for a wider range of angles of attack as shown in Figure 21. Excellent agreement is observed between the analytic relations and CBAERO.

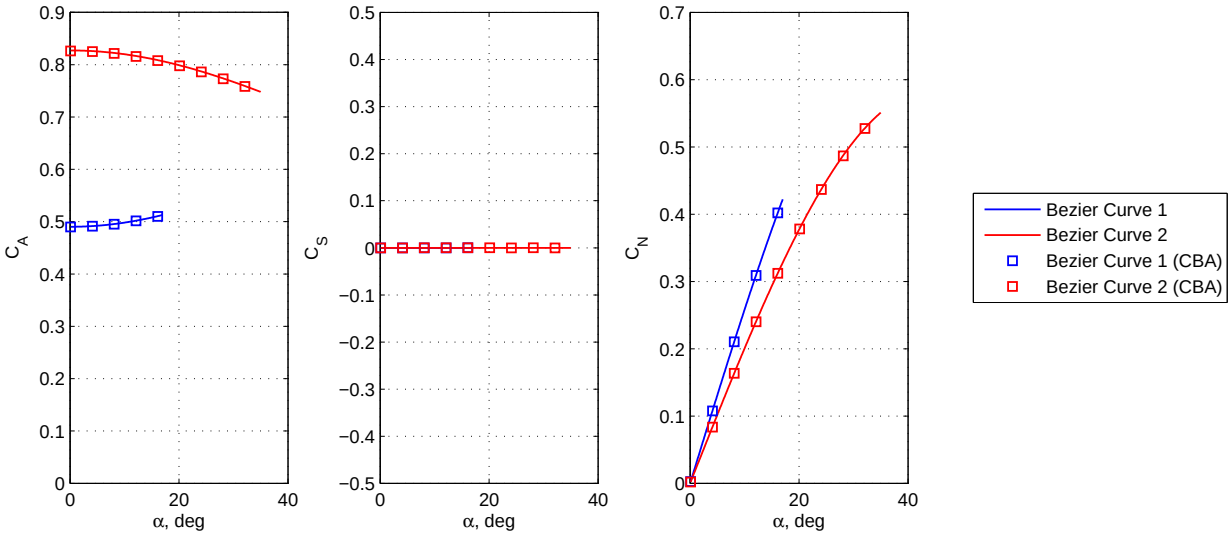

Figure 21. Validation of Unshadowed Bezier Curves of Revolution.

VIII. Potential Applications of Analytic Aerodynamics

The analytic aerodynamic relations were originally developed to reduce computational requirements, compared to panel methods and CFD, for the conceptual design of entry vehicles. This allows for rapid aerodynamic analysis when performing trade studies or shape optimization. Additionally, the evaluation of the aerodynamics module is nearly instantaneous and can be the fastest module among all disciplines in conceptual design.

Typically during conceptual design, optimal trajectories are identified to determine the nominal aerodynamic performance requirements of the entry vehicle, such as peak L/D and ballistic coefficient. A vehicle can then be constructed to meet these aerodynamic constraints as well as other geometric constraints. However, in some cases, high performance entry trajectories are not flown at a constant angle of attack, resulting in L/D and ballistic coefficient varying throughout the trajectory. Consequently, an iterative process must be performed until convergence between vehicle shape and time-varying aerodynamic performance required by the trajectory is observed. Furthermore, within the trajectory optimization process, the mapping of vehicle shape to aerodynamic performance is largely performed using tables of aerodynamic coefficients as a function of angle of attack and sideslip.

If direct methods are used for entry trajectory optimization, then the addition of shape design parameters would simply augment the overall optimization problem.[27,28] In this case, the analytic aerodynamic relations would be directly integrated into the trajectory simulation, dramatically reducing the computational requirements of evaluating the aerodynamic coefficients along each candidate trajectory. Additionally, any constraints on the shape parameters would constrain the search domain of the direct optimization method.

If indirect methods are used to perform trajectory optimization, then analytic mapping of vehicle shape to aerodynamic performance would allow the indirect method to perform simultaneous trajectory and vehicle shape optimization. The analytic aerodynamic relations could be directly integrated into the equations of motion, modeling the varying L/D and ballistic coefficient throughout the trajectory. Additionally, constraints on vehicle shape such as diameter and volume can be directly integrated into the augmented objective function. This can be performed in a way identical to the incorporation of interior point constraints.[29]

To date, the concept of predictor-corrector guidance algorithms have largely been confined to academic studies. This is partially due to the large tables of aerodynamic coefficients that must be interpolated onboard for various angles of attack and sideslip. PredGuid, planned for incorporation into the Orion command module for lunar return, will implement a predictor-corrector in the onboard guidance of a flight vehicle. The predictor-corrector of PredGuid solves for a constant bank angle solution to perform a skip during the first entry in order to land off the coast of California.[30] The analytic hypersonic relations developed in this investigation could substitute the large aerodynamic tables, allowing real-time onboard propagation of

trajectories using angle of attack, bank, and sideslip for onboard predictor-corrector guidance algorithms.

The propagation of trajectories, either onboard in predictor-corrector studies or during trajectory optimization, generally ignores the shape change experienced by the vehicle throughout the entry trajectory. Instead, ablation studies are usually performed after the design of the trajectory and vehicle in order to estimate the thermal protection system thickness and mass. However, analytic aerodynamic relations would enable the modeling of shape change due to ablation during trajectory propagation.

IX. Conclusions

Hypersonic force and moment coefficients can be obtained through the use of Newtonian flow theory in which a surface integration of the pressure coefficient is performed. The advent of the digital computer has resulted in widespread adoption of panel methods in which the surface integration is numerically approximated through surface paneling. Paneling techniques allow for the evaluation of complex geometries. However, many entry vehicle geometries used today are not complex and are derived from the superposition of basic shapes.

In this investigation, an automated process has been developed to evaluate the surface integration of pressure coefficient analytically. Analytic relations for force coefficients, moment coefficients, and stability derivatives were developed for basic shapes including sharp cones, spherical segments, flat plates, and cylindrical segments. Each basic shape was parametrized according to the characteristics of the shape. Consequently, only one set of analytic relations were developed for each basic shape. These analytic relations account for shadowed and unshadowed angles of attack and sideslip. The basic shapes can be superpositioned to construct commonly used entry vehicles, such as sphere-cones and biconics. The analytic relations for force coefficients, moment coefficients, and stability derivatives for all of these shapes were verified using CBAERO or another paneling code. Evaluation of the resulting analytic relations is nearly instantaneous and is orders of magnitude faster than paneling codes. An example biconic shape design was performed to maximize payload packaging capability while maintaining required aerodynamic performance. The entire design process that originally would require hours using panel methods was executed in minutes using analytic relations.

In order to obtain the analytic aerodynamics for more general bodies of revolution, relations were developed for second-order Bezier curves of revolution at unshadowed total angles of attack. These relations were parametrized by the location of control nodes associated with the Bezier curve. Aerodynamic force coefficients were validated using CBAERO. This served as an initial step in addressing the limits in generality that can be achieved with analytic relations. The resulting analytic equations of basic shapes and Bezier curves of revolution could dramatically impact integrated vehicle and trajectory design, trajectory propagation for onboard guidance, and aerodynamic modeling of shape change due to ablation.

References

[1]Newton, I., *Principia - Motte's Translation Revised*, University of California Press, 1946.

[2]Anderson, J. D., *Hypersonic and High Temperature Gas Dynamics*, AIAA, 1989.

[3]Cummings, R. M. and Yang, H.-T., "Lester Lees and Hypersonic Aerodynamics," *Journal of Spacecraft and Rockets*, Vol. 40, No. 4, 2003.

[4]Bonner, E., Clever, W., and Dunn, K., "Aerodynamic Preliminary Analysis System II: Part I Theory," *NASA-CR-165627*, Apr. 1981.

[5]Smyth, D. N. and Loo, H. C., "Analysis of Static Pressure Data from 1/12-scale Model of the YF-12A. Volume 3: The MARK IVS Supersonic-Hypersonic Arbitrary Body Program, User's Manual," *NASA-CR-151940*, Oct. 1981.

[6]Cunningham, M., "Hypersonic Aerodynamics for an Entry Research Vehicle," *Journal of Spacecraft and Rockets*, Vol. 24, No. 2, 1987.

[7]Kinney, D. J., "Aero-Thermodynamics for Conceptual Design," AIAA-2004-31-962, *42nd AIAA Aerospace Sciences Meeting and Exhibit*, Reno, NV, 5-8 Jan. 2004.

[8]Hoffman, S. J. and Kaplan, D. I., "Human Exploration of Mars: The Reference Mission of the NASA Mars Exploration Study Team," *NASA Special Publication 6107*, July 1997.

[9]Drake, B. G., "Reference Mission Version 3.0 Addendum to the Human Exploration of Mars: The Reference Mission of the NASA Mars Exploration Study Team," *NASA Special Publication 6107-ADD*, June 1998.

[10]Steinfeldt, B., Theisinger, J., Korzun, A., Clark, I., Grant, M., and Braun, R., "High Mass Mars Entry Descent and Landing Architecture Assessment," AIAA 2009-6684, *AIAA Space 2009*, Pasadena, CA, 14 - 17 Sept. 2009.

[11]Desai, P., Lyons, D., Tooley, J., and Kangas, J., "Entry, Descent, and Landing Operations Analysis for the Stardust Entry Capsule," *Journal of Spacecraft and Rockets*, Vol. 45, No. 6, 2008.

[12]Desai, P. and Lyons, D., "Entry, Descent, and Landing Operations Analysis for the Genesis Entry Capsule," *Journal of Spacecraft and Rockets*, Vol. 45, No. 1, 2008.

[13]Kinney, D. J. and Bowles, J. V., "Conceptual Design of a 'SHARP'-CTV," AIAA 2001-2887, *35th AIAA Thermophysics Conference*, Anaheim, CA, 11-14 Jun. 2001.

[14]Wells, W. and Armstrong, W., "Tables of Aerodynamic Coefficients Obtained From Developed Newtonian Expressions for Complete and Partial Conic and Spheric Bodies at Combined Angles of Attack and Sideslip with Some Comparisons with Hypersonic Experimental Data," *NASA TR R-127*, 1962.

[15]Elsgloc, L. D., *Calculus of Variations*, Dover Publications, Inc., 2007.

[16]Eggers, A. J., Resnikoff, M. M., and Dennis, D. H., "Bodies of Revolution Having Minimum Drag at High Supersonic Airspeeds," *NACA TR-1306*, 1957.

[17]Auman, L. M. and Wilks, B., "Supersonic and Hypersonic Minimum Drag for Bodies of Revolution," *AIAA 21st Applied Aerodynamics Conference*, Orlando, FL, 23-26 Jun. 2003.

[18]Rainey, R. W., "Working Charts for Rapid Prediction of Force and Pressure Coefficients on Arbitrary Bodies of Revolution by Use of Newtonian Concepts," *NASA TN D-176*, 1959.

[19]Regan, F. J. and Anandakrishnan, S. M., *Dynamics of Atmospheric Re-Entry*, AIAA, 1993.

[20]Grimminger, G., Williams, E. P., and Young, G. B. W., "Lift on Inclined Bodies of Revolution in Hypersonic Flow," *Journal of the Aeronautical Sciences*, Vol. 17, No. 11, 1950.

[21]Margolis, K., "Theoretical Evaluation of the Pressures, Forces, and Moments at Hypersonic Speeds Acting on Arbitrary Bodies of Revolution Undergoing Separate and Combined Angle-of-Attack and Pitching Motions," *NASA TN D-652*, 1961.

[22]Theisinger, J. E. and Braun, R. D., "Multi-Objective Hypersonic Entry Aeroshell Shape Optimization," *Journal of Spacecraft and Rockets*, Vol. 46, No. 5, 2009.

[23]Kinney, D. J., "Aerodynamic Shape Optimization of Hypersonic Vehicles," AIAA 2006-239, *44th AIAA Aerospace Sciences Meeting and Exhibit*, Reno, NV, 9-12 Jan. 2006.

[24]Mathematica, Ver. 7, Wolfram Research, Champaign, IL.

[25]Maple, Ver. 13, Waterloo Maple Inc., Waterloo, Ontario, Canada.

[26]Rogers, D. F., *An Introduction to NURBS: With Historical Perspective*, Academic Press, London, 2001.

[27]Grant, M. J. and Mendeck, G. F., "Mars Science Laboratory Entry Optimization Using Particle Swarm Methodology," AIAA 2007-6393, *AIAA Atmospheric Flight Mechanics Conference and Exhibit*, Hilton Head, SC, 20-23 Aug. 2007.

[28]Lafleur, J. and Cerimele, C., "Mars Entry Bank Profile Design for Terminal State Optimization," AIAA 2008-6213, *AIAA Atmospheric Flight Mechanics Conference and Exhibit*, Honolulu, HI, 18-21 Aug. 2008.

[29]Bryson, A. E. and Ho, Y.-C., *Applied Optimal Control*, Taylor and Francis, 1975.

[30]Putnam, Z. R., Braun, R. D., Bairstow, S. H., and Barton, G. H., "Improving Lunar Return Entry Footprints Using Enhanced Skip Trajectory Guidance," AIAA-2006-7438, *Space 2006*, San Jose, CA, 19-21 Sep. 2006.